Radio Science, Volume 26, Number 6, Pages 1393–1401, November–December 1991

Electromagnetic scattering for multilayered sphere: Recursive algorithms

Z. S. Wu and Y. P. Wang

Department of Physics, Xidian University, Xi'an Shaanxi, People's Republic of China

(Received March 27, 1990; revised September 24, 1990; accepted March 25, 1991.)

We have proposed more stable and accurate recursing equations and a computing procedure to calculate scattering coefficients for a multilayered sphere. The procedure involves three logarithmic derivatives of Ricatti–Bessel functions $\psi_n'(z)/\psi_n(z)$, $\chi_n'(z)/\chi_n(z)$, and $\xi_n'(z)/\xi_n(z)$, as well as the ratio $\psi_n(z)/\chi_n(z)$. The asymptotic behavior, stability, and accuracy of the procedure and scattering coefficients a_n and b_n are discussed for any complex refractive indices. This procedure can be used for large and small inhomogeneous spherical particles.

1. INTRODUCTION

The formulation of the electromagnetic scattering of a coated sphere was first derived by *Aden and Kerker* [1951] and discussed in detail [*Kerker*, 1969; *Toon and Ackerman*, 1981; *Bohren and Huffman*, 1983]. This work was involved in many areas of scientific research and applications. However, some difficulties in computation were encountered in using Kerker's equations directly, in which the magnitudes of spherical Bessel functions increase exponentially with the argument and can easily exceed the capacity of a computer. Large errors, resulting from the removal of higher–order terms in expansions for the scattering field, may occur in using the upward recursion to calculate the Ricatti–Bessel functions. Similar difficulties were reported in calculation of electromagnetic (em) scattering for the homogeneous sphere numerically. In order to circumvent these difficutties, several authors succeeded in recasting the problems into suitable forms and presented the computational algorithms [*Dave*, 1968; *Kattawar and Plass*, 1976; *Wiscombe*, 1980; *Toon and Ackerman*, 1981].

Kerker [1969] generalized the aforementioned problems to a multilayered sphere, in which the refractive index varies continuously from the center to the outer surface, and presented the scattering coefficients a_n and b_n in a form of determinants. *Bhandari* [1985] proposed the calculational procedure for scattering coefficients in directly using Kerker's equations. However, the forms and computational schemes used are complex algorithms. In this paper, Kerker's equations for the scattering coefficients have eventually been transformed into simple and suitable calculational forms, which are derived directly by means of the iterative procedure. This procedure involves three logarithmic derivatives of Ricatti–Bessel functions $\psi_n'(z)/\psi_n(z)$, $\chi_n'(z)/\chi_n(z)$, and $\xi_n'(z)/\xi_n(z)$, as well as the ratio $\psi_n(z)/\chi_n(z)$. And we discuss in detail the asymptotic form of these functions and their influence on the calculation of the scattering coefficients. Finally, the various tests show that the equations presénted and the iterative method are stable and accurate for any complex refractive indices and for both large and small particles.

Paper number 91RS01192.
0048-6604/91/91RS-01192$08.00

2. SCATTERING COEFFICIENTS

The electromagnetic scattering by a multilayered dielectric sphere is depicted in Figure 1. The value m_j is the refractive index of the material in j th region relative to the refractive index m_g of the surrouding medium, in which the sphere is embeded. The corresponding size parameter $x_j = kr_j = 2\pi r_j/\lambda$, where r_j is the various radii and λ is the wavelength of the incident plane wave in free space. Suppose the electric field is an incident plane wave $E_i = E_o \exp(ikz)$. The incident wave field may be expanded in an infinite series of vector spherical harmonics as follows:

$$\vec{E}_i = \sum_{n=1}^{\infty} E_n(\vec{M}^{(1)}_{on} - i\vec{N}^{(1)}_{en}) \tag{1}$$

$$\vec{H}_i = -\frac{k}{\omega\mu} \sum_{n=1}^{\infty} E_n(\vec{M}^{(1)}_{en} + i\vec{N}^{(1)}_{on}) \tag{2}$$

where $E_n = i^n E_o(2n+1)/n(n+1)$, k and μ are the propagation constant and the permeability of the surrouding medium, respectively. According to the radiation con-

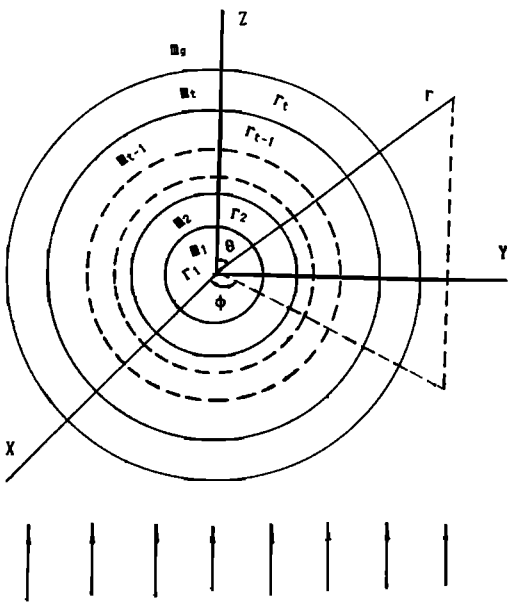

Fig. 1. Geometry for scattering of a multilayered sphere.

dition of an outgoing wave and asymptotic behavior of the spherical Bessel functions, only $h_n^{(1)}$ should be retained in the radial function. Therefore the expansion of $\vec{E}_s$ and $\vec{H}_s$ are

$$\vec{E}_s = \sum_{n=1}^{\infty} E_n (ia_n \vec{N}_{e1n}^{(3)} - b_n \vec{M}_{o1n}^{(3)}) \tag{3}$$

$$\vec{H}_s = -\frac{k}{\omega\mu} \sum_{n=1}^{\infty} E_n (ib_n \vec{N}_{o1n}^{(3)} + a_n \vec{M}_{e1n}^{(3)}) \tag{4}$$

Since the wave field must be finite at the origin, we take j_n as the appropriate spherical Bessel function in the radial functions for the vector harmonics inside the core sphere. Thus the expansion of field $(\vec{E}_1, \vec{H}_1)$ is

$$\vec{E}_1 = \sum_{n=1}^{\infty} E_n (c_n^{(1)} \vec{M}_{o1n}^{(1)} - id_n^{(1)} \vec{N}_{e1n}^{(1)}) \tag{5}$$

$$\vec{H}_1 = -\frac{k_1}{\omega\mu_1} \sum_{n=1}^{\infty} E_n (d_n^{(1)} \vec{M}_{e1n}^{(1)} + ic_n^{(1)} \vec{N}_{o1n}^{(1)}) \tag{6}$$

However, in the region $r_1 \leq r \leq r_t (r_1 \neq 0)$, both spherical Bessel functions j_n *and* y_n are finite. As a consequence, the expansions of the field in the jth region ($j = 2, 3, \ldots, t$) are

$$\vec{E}_j = \sum_{n=1}^{\infty} E_n (c_n^{(j)} \vec{M}_{o1n}^{(1)} - id_n^{(j)} \vec{N}_{o1n}^{(1)} + f_n^{(j)} \vec{M}_{e1n}^{(2)} - ig_n^{(j)} \vec{N}_{e1n}^{(2)}) \tag{7}$$

$$\vec{H}_j = -\frac{k_j}{\omega\mu_j} \sum_{n=1}^{\infty} E_n (d_n^{(j)} \vec{M}_{e1n}^{(1)} + ic_n^{(j)} \vec{N}_{o1n}^{(1)} + g_n^{(j)} \vec{M}_{e1n}^{(2)} + if_n^{(j)} \vec{N}_{e1n}^{(2)}) \tag{8}$$

In the above formulae the spherical harmonics functions are as follows [*Stratton*, 1941; *Bohren and Huffman*, 1983]:

$$\begin{Bmatrix} \vec{M}_{o1n} \\ \vec{M}_{e1n} \end{Bmatrix} = Z_n(kr) \cdot \pi_n(\cos\theta) \begin{Bmatrix} \cos\varphi \\ -\sin\varphi \end{Bmatrix} \hat{e}_\theta - Z_n(kr) \cdot \tau_n(\cos\theta) \begin{Bmatrix} \sin\varphi \\ \cos\varphi \end{Bmatrix} \hat{e}_\varphi \tag{9a}$$

$$\begin{Bmatrix} \vec{N}_{o1n} \\ \vec{N}_{e1n} \end{Bmatrix} = n(n+1)\frac{Z_n(kr)}{kr} \pi_n(\cos\theta) \begin{Bmatrix} \sin\varphi \\ \cos\varphi \end{Bmatrix} \hat{e}_r + \frac{[krZ_n(kr)]'}{kr} \cdot \tau_n(\cos\theta) \begin{Bmatrix} \sin\varphi \\ \cos\varphi \end{Bmatrix} \hat{e}_\theta + \frac{[krZ_n(kr)]'}{kr} \cdot \pi_n(\cos\theta) \begin{Bmatrix} \cos\varphi \\ -\sin\varphi \end{Bmatrix} \hat{e}_\varphi \tag{9b}$$

The superscripts 1, 2, and 3 for vector spherical harmonics indicate that the radial dependence of the functions are j_n, y_n and $h_n^{(1)}$, respectively. The angle–dependent function π_n and τ_n are

$$\pi_n = \frac{P_n^{(1)}(\cos\theta)}{\sin\theta} \qquad \tau_n = \frac{dP_n^{(1)}(\cos\theta)}{d\theta} \tag{10}$$

The propagation constant $k_j = 2\pi m_j / \lambda$, and μ_j is the permeability in the jth region. Let us assume for simplicity that $\mu_1 = \mu_2 = \cdots = \mu_t = \mu$. The boundary conditions for the interface in different regions are

$$\begin{aligned} &(\vec{E}_{j+1} - \vec{E}_j) \times \hat{e}_r = 0, \ (\vec{H}_{j+1} - \vec{H}_j) \times \hat{e}_r = 0 \\ &\qquad r = r_j \qquad (j = 1,2,\ldots,t-1) \\ &(\vec{E}_s + \vec{E}_t - \vec{E}_t) \times \hat{e}_r = 0, \ (\vec{H}_s + \vec{H}_t - \vec{H}_t) \times \hat{e}_r = 0 \\ &\qquad r = r_t \end{aligned} \tag{11}$$

In addition to $f_n^{(1)} = g_n^{(1)} = 0$, two sets of $2t$ simultaneous equations of unknown coefficients a_n, b_n, $c_n^{(j)}$, $d_n^{(j)}$, $f_n^{(j)}$, $g_n^{(j)}$ are set up,

$$d_n^{(2)} m_1 \psi_n'(m_2 x_1) - g_n^{(2)} m_1 \chi_n'(m_2 x_1) - d_n^{(1)} m_2 \psi_n'(m_1 x_1) = 0 \tag{12a}$$

$$d_n^{(2)} \psi_n(m_2 x_1) - g_n^{(2)} \chi_n(m_2 x_1) - d_n^{(1)} \psi_n(m_1 x_1) = 0 \tag{12b}$$

$$d_n^{(j)} m_{j-1} \psi_n'(m_j x_{j-1}) - g_n^{(j)} m_{j-1} \chi_n'(m_j x_{j-1}) - d_n^{(j-1)} m_j \psi_n'(m_{j-1} x_{j-1}) + g_n^{(j-1)} m_j \chi_n'(m_{j-1} x_{j-1}) = 0 \tag{12c}$$

$$d_n^{(j)} \psi_n(m_j x_{j-1}) - g_n^{(j)} \chi_n(m_j x_{j-1}) - d_n^{(j-1)} \psi_n(m_{j-1} x_{j-1}) + g_n^{(j-1)} \chi_n(m_{j-1} x_{j-1}) = 0 \tag{12d}$$

$$a_n m_t \xi_n'(x_t) - m_t \psi_n'(x_t) + d_n^{(t)} \psi_n'(m_t x_t) - g_n^{(t)} \chi_n'(m_t x_t) = 0 \tag{12e}$$

$$a_n\xi_n(x_t)-\psi_n(x_t)+d_n^{(t)}\psi_n(m_tx_t)-g_n^{(t)}\chi_n(m_tx_t)=0 \tag{12f}$$

$$c_n^{(2)}m_1\psi_n(m_2x_1)-f_n^{(2)}m_1\chi_n(m_2x_1)-c_n^{(1)}m_2\psi_n(m_1x_1)=0 \tag{13a}$$

$$c_n^{(2)}\psi_n'(m_2x_1)-f_n^{(2)}\chi_n'(m_2x_1)-c_n^{(1)}\psi_n'(m_1x_1)=0 \tag{13b}$$

$$c_n^{(j)}m_{j-1}\psi_n(m_jx_{j-1})-f_n^{(j)}m_{j-1}\chi_n(m_jx_{j-1})-c_n^{(j-1)}m_j\psi(m_{j-1}x_{j-1})+f_n^{(j-1)}m_j\chi_n(m_{j-1}x_{j-1})=0 \tag{13c}$$

$$c_n^{(j)}\psi_n'(m_jx_{j-1})-f_n^{(j)}\chi_n'(m_jx_{j-1})-c_n^{(j-1)}\psi_n'(m_{j-1}x_{j-1})+f_n^{(j-1)}\chi_n'(m_{j-1}x_{j-1})=0 \tag{13d}$$

$$b_nm_t\xi_n(x_t)-m_t\psi_n(x_t)+c_n^{(t)}\psi_n(m_tx_t)-f_n^{(t)}\chi_n(m_tx_t)=0 \tag{13e}$$

$$b_n\xi_n'(x_t)-\psi_n'(x_t)+c_n^{(t)}\psi_n'(m_tx_t)-f_n^{(t)}\chi_n'(m_tx_t)=0 \tag{13f}$$

where Ricatti–Bessel functions $\psi_n(z)=zj_n(z)$, $\chi_n(z)=-zy_n(z)$, and $\xi_n(z)=zh_n^{(1)}(z)=\psi_n(z)-i\chi_n(z)$. Let $A_n^{(j)}=g_n^{(j)}/d_n^{(j)}$ and $B_n^{(j)}=f_n^{(j)}/c_n^{(j)}$, then $A_n^{(1)}=B_n^{(1)}=0$. In this case we have to solve a pair of equations associated with $d_n^{(j)}$ and $g_n^{(j)}$, or $c_n^{(j)}$ and $f_n^{(j)}$ in their regular order. This procedure leads to analytically recurrent expressions for $A_n^{(j)}$ and $B_n^{(j)}$. For example, the coefficient $A_n^{(j)}$ and scattering coefficient a_n can be expressed as

$$A_n^{(2)}=\frac{m_2\psi_n(m_2x_1)\psi_n'(m_1x_1)-m_1\psi_n'(m_2x_1)\psi_n(m_1x_1)}{m_2\chi_n(m_2x_1)\psi_n'(m_1x_1)-m_1\chi_n'(m_2x_1)\psi_n(m_1x_1)}$$

$$A_n^{(j)}=\frac{m_j\psi_n(m_jx_{j-1})H_n^a(m_{j-1}x_{j-1})-m_{j-1}\psi_n'(m_jx_{j-1})}{m_j\chi_n(m_jx_{j-1})H_n^a(m_{j-1}x_{j-1})-m_{j-1}\chi_n'(m_jx_{j-1})} \tag{14}$$

$$H_n^a(m_jx_j)=\frac{\psi_n'(m_jx_j)-A_n^{(j)}\chi_n'(m_jx_j)}{\psi_n(m_jx_j)-A_n^{(j)}\chi_n(m_jx_j)} \tag{15}$$

$$a_n=\frac{\psi_n(x_t)H_n^a(m_tx_t)-m_t\psi_n'(x_t)}{\xi_n(x_t)H_n^a(m_tx_t)-m_t\xi_n'(x_t)} \tag{16}$$

By comparing the two sets of $2t$ simultaneous equations (12) and (13), ($j=1, 2, \cdots, t$), functions $B_n^{(j)}$ and $H_n^b(m_jx_j)$ are derived directly from $A_n^{(j)}$ and $H_n^a(m_jx_j)$ by exchanging the relative refractive indices m_{j-1} and m_j in (14) and by replacing $A_n^{(j)}$ with $B_n^{(j)}$ in (15). Thus, another scattering coefficient b_n is expressed as

$$b_n=\frac{m_t\psi_n(x_t)H_n^b(m_tx_t)-\psi_n'(x_t)}{m_t\xi_n(x_t)H_n^b(m_tx_t)-\xi_n'(x_t)} \tag{17}$$

In a way similar to that for the case of a single homogeneous sphere, one can calculate the various scatting cross sections and the amplitude of scattering matrix elements by means of the scattering coefficients a_n and b_n from (16) and (17).

3. COMPUTATIONAL SCHEME

To compute a_n and b_n, we have to select specific algorithms, because the magnitude of a spherical Bessel function increases exponentially with the module of the complex argument and may easily exceed the capicity of a computer. In addition, the higher-order terms in the expansions for the scattering field are subject to large calculating error and accumulative error, especially when the size parameter of a multilayered sphere is larger. However, both the ratios and the logarithmic derivatives of the Ricatti–Bessel functions are bounded as the total size parameter becomes large and the core size becomes small. To remove these difficulties, equations (14)–(17) are refomulated into more convenient forms for computation, which are as follows:

$$A_n^{(1)}=0,\quad H_n^a(m_1x_1)=D_n^{(1)}(m_1x_1)$$

$$A_n^{(j)}=\frac{\psi_n(m_jx_{j-1})}{\chi_n(m_jx_{j-1})}\cdot\frac{m_jH_n^a(m_{j-1}x_{j-1})-m_{j-1}D_n^{(1)}(m_jx_{j-1})}{m_jH_n^a(m_{j-1}x_{j-1})-m_{j-1}D_n^{(2)}(m_jx_{j-1})} \tag{18}$$

$$H_n^a(m_jx_j)=\frac{[\psi_n(m_jx_j)/\chi_n(m_jx_j)]D_n^{(1)}(m_jx_j)}{\psi_n(m_jx_j)/\chi_n(m_jx_j)-A_n^{(j)}}-\frac{A_n^{(j)}D_n^{(2)}(m_jx_j)}{\psi_n(m_jx_j)/\chi_n(m_jx_j)-A_n^{(j)}}$$

$$a_n=\frac{\psi_n(x_t)}{\xi_n(x_t)}\cdot\frac{H_n^a(m_tx_t)-m_tD_n^{(1)}(x_t)}{H_n^a(M_tx_t)-m_tD_n^{(3)}(x_t)} \tag{19}$$

$$B_n^{(1)}=0\ ,\quad H_n^b(m_1x_1)=D_n^{(1)}(m_1x_1)$$

$$B_n^{(j)}=\frac{\psi_n(m_jx_{j-1})}{\chi_n(m_jx_{j-1})}\cdot\frac{m_{j-1}H_n^b(m_{j-1}x_{j-1})-m_jD_n^{(1)}(m_jx_{j-1})}{m_{j-1}H_n^b(m_{j-1}x_{j-1})-m_jD_n^{(2)}(m_jx_{j-1})} \tag{20}$$

$$H_n^b(m_j-x_j)=\frac{[\psi_n(m_jx_j)/\chi_n(m_jx_j)]D_n^{(1)}(m_jx_j)}{\psi_n(m_jx_j)/\chi_n(m_jx_j)-B_n^{(j)}}-\frac{B_n^{(j)}D_n^{(2)}(m_jx_j)}{\psi_n(m_jx_j)/\chi_n(m_jx_j)-B_n^{(j)}}$$

$$b_n=\frac{\psi_n(X_t)}{\xi_n(X_t)}\cdot\frac{m_tH_n^b(m_tx_t)-D_n^{(1)}(X_t)}{m_tH_n^b(m_tx_t)-D_n^{(3)}(X_t)} \tag{21}$$

where $D_n^{(1)}(z)=\psi_n'(z)/\psi_n(z)$, $D_n^{(2)}(z)=\chi_n'(z)/\chi_n(z)$, and $D_n^{(3)}(z)=\xi_n'(z)/\xi_n(z)$ are the logarithmic derivatives of Ricatti–Bessel functions. In the above reccurent formulae there are only three logarithmic derivative functions and the ratio of Ricatti–Bessel functions

$\psi_n(z)/\chi_n(z)(\psi_n(z)/\xi_n(z)$ is expressed in $\psi_n(z)/\chi_n(z))$ From the well–known recurrence relations of the Ricatti–Bessel function $B_n(z)(B_n(z)$ is $\psi_n(z)$ or $\chi_n(z)$, including $\xi_n(z))$

$$B_n'(z)+\frac{n}{z}B_n(z)=B_{n-1}(z) \tag{22}$$

$$B_n(z)=\frac{n}{z}B_{n-1}(z)-B_{n-1}'(z) \tag{23}$$

The logarithmic derivatives of them satisfy an identical recurrence relation

$$D_n^{(l)}=1/[n/z-D_{n-1}^{(l)}]-n/z \qquad l=1,\ 2,\ 3 \tag{24}$$

and their initial values are

$$D_n^{(1)}(z)=\cos z/\sin z \tag{25}$$

$$D_n^{(2)}(z)=-\sin z/\cos z \tag{26}$$

$$D_n^{(3)}(z)=i \tag{27}$$

One could also derive the recurrence relation for ratio $\psi_n(z)/\chi_n(z)$ in (23)

$$\frac{\psi_n(z)}{\chi_n(z)}=\frac{\psi_{n-1}(z)}{\chi_{n-1}(z)}\cdot\frac{[D_n^{(2)}(z)+n/z]}{[D_n^{(1)}(z)+n/z]} \tag{28}$$

$$\psi_o(z)/\chi_o(z)=\sin z/\cos z \tag{29}$$

Similarly, the ratio $\psi_n(z)/\xi_n(z)$ is expressed as

$$\frac{\psi_n(z)}{\xi_n(z)}=\frac{\psi_{n-1}(z)}{\xi_{n-1}(z)}\cdot\frac{[D_n^{(3)}(z)+n/z]}{[D_n^{(1)}(z)+n/z]} \tag{30}$$

$$\psi_o(z)/\xi_o(z)=\sin z/[\sin z-i\cos z] \tag{31}$$

In addition, we must pay great attention to the fact that the Ricatti–Bessel functions with large complex argument cannot be directly evaluated in upward recursion, because they are not bounded for a large complex argument. We have to rewrite (26), (29), and (31), for example,

$$D_o^{(2)}(z)=i\frac{1-(\cos 2x+i\sin 2x)\exp(-2y)}{1+(\cos 2x+i\sin 2x)\exp(-2y)} \tag{32}$$

where $z=x+iy$. Since $y>0$, the calculation does not cause overflow whenever $|z|$ is large. The functions $\psi_o(z)/\chi_o(z)$ and $\psi_o(z)/\xi_o(z)$ can be treated in the similar way.

4. ASYMPTOTIC BEHAVIOR OF $D_n^{(1)}(z)$, $D_n^{(2)}(z)$, $D_n^{(3)}(z)$, AND $\psi_n(z)/\chi_n(z)$

We must examine carefully the behavior of the logarithmic derivatives of Ricatti–Bessel functions and the ratio of spherical Bessel and Neumann functions. As discussed by *Kattawar and Plass* [1967] as well as *Dave* [1969], the calculation of $D_n^{(1)}(z)$ by upward recursion is numerically unstable when $n \gg N_{stop}$ (N_{stop} will be discussed below). On the other hand, $D_n^{(1)}(z)$ is always calculated by downward recurrence formula and the calculation is started from $n \gg N_{stop}$. The computational error decreases at each step and numerical results rapidly converge to the correct values. Let ε_n be the error in the approximate numerical value of the true value of $D_n^{(1)}(z)$. From the downward recurrence relation (rewrite equation (24)),

$$D_{n-1}^{(1)}(z)=n/z-[D_n^{(1)}(z)+n/z]^{-1} \tag{33}$$

there is

$$D_{n-1}^{(1)}(z)+\varepsilon_{n-1}(z)=n/z-[D_n^{(1)}(z)+\varepsilon_n(z)+n/z]^{-1}$$

When $\gg |z|$,

$$|\varepsilon_{n-1}(z)| \sim |\varepsilon_n(z)|/[(2n+1)/z] \ll |\varepsilon_n(z)|$$

We choose a value of the largest–order term $N_{max}=N_{stop}+15$, [*Bohren and Huffman*, 1983] which is the cutoff in the series expansion of (3) and (4), and set $D_n^{(1)}(z)$ arbitrarily to zero when $n=N_{max}+1$ in downward recursion. N_{stop} is the order term which is closest to Max $(x_t+4x_t^{1/3}+2, m_j x_j)(j=1, \cdots, t-1)$. This criterion was also discussed by *Dave* [1968] and *Wiscombe* [1980]. $D_n^{(2)}(z)$ may be calculated by upward recursing formulae (24)and (27), and the numerical error rapidly decreases with increasing n [*Kattawar and Plass*, 1967; *Toon and Ackerman*, 1981]. In this paper we discuss mainly the asymptotic behavior of $D_n^{(2)}(z)$ and the ratio $\psi_n(z)/\chi_n(z)$, including the ratio $\psi_n(z)/\xi_n(z)$. The Ricatti–Bessel function $\chi_n(z)$ is computed by using upward recurrence [*Abramowitz and Stegun*, 1964], but its magnitude increases exponentially with the argument and may easily exceed the capacity of modern computers. From the relation of the Ricatti–Bessel functions, $D_n^{(2)}(z)$ is expressed as

$$D_n^{(2)}(z)=[\psi_n'(z)-\xi_n'(z)]/[\psi_n(z)-\xi_n(z)]$$

$$=\frac{[\psi_n(z)/\xi_n(z)\cdot D_n^{(1)}(z)-D_n^{(3)}(z)]}{[\psi_n(z)/\xi_n(z)-1]} \tag{34}$$

The ratio $\psi_n(z)/\xi_n(z)$ may be computed by using iterative formula (30). When $n \gg |z|$, both the real and the imaginary parts of $\psi_n(z)/\xi_n(z)$ fall rapidly and approach zero (see Table 1 and Figure 3*a*). Thus $D_n^{(2)}(z)=D_n^{(3)}(z) \approx -n/z \approx -D_n^{(1)}(z)$ as $n>N_{stop}$. In our code, $D_n^{(2)}(z)$ and $D_n^{(3)}(z)$ can be computed using upward recurrence.

The above behavior of $D_n^{(1)}(z)$ ($l=1$, 2, and 3) is illustrated in Table 1 and in Figure 2. The example in Table 1 is the nucleated blood cell in an aqueous solution irradiated by a He–Ne laser and the corresponding size paramater of cytoplasm z is equal to (84.0, 0.4). The ratio $\psi_n(z)/\xi_n(z)$ is also shown in Table 1. The illustrative example in Figure 2 is a water–coated ice particle in milliwave region. The refractive index of water

TABLE 1. Nucleated Blood Cell in an Aqueous Solution

n	$D_n^{(1)}(z)$	$D_n^{(2)}(z)$	$D_n^{(3)}(z)$	$\psi_n(z)/\xi_n(z)$
0	(−0.70593, −0.62872)	(0.78997, $-0.70356\times10^{+1}$)	(0.00000, 1.0000)	(0.58361, $-0.11096\times10^{+1}$)
30	(-0.52009×10^{-1}, −0.33324)	(0.39314, $-0.25449\times10^{+1}$)	(-0.15760×10^{-2}, 0.93181)	($0.15453\times10^{+1}$, −0.13256)
60	(0.79715, $-0.22573\times10^{+1}$)	(-0.71869×10^{-1}, −0.18994)	(-0.99318×10^{-2}, 0.69425)	(−0.35277, 0.17825)
84	(0.23532, −0.01732)	(−0.18670, -0.94420×10^{-2})	(−0.12741, 0.17311)	(0.13235, 0.43504)
90	(0.43753, -0.12261×10^{-1})	(−0.34323, -0.17218×10^{-1})	(−0.34633, 0.28863×10^{-1})	(-0.45216×10^{-2}, 0.14744×10^{-5})
99	(0.65463, -0.10192×10^{-1})	(−0.61282, 0.11020×10^{-1})	(−0.61282, 0.11022×10^{-1})	(-0.94077×10^{-6}, 0.16939×10^{-5})
110	(0.86560, -0.96687×10^{-2})	(−0.84023, 0.97714×10^{-2})	(−0.84023, -0.97714×10^{-2})	(-0.31012×10^{-12}, 0.38070×10^{-12})
111	(0.87245, -0.99585×10^{-2})	(−0.85881, 0.97300×10^{-2})	(−0.85881, 0.97300×10^{-2})	(-0.66575×10^{-13}, 0.79294×10^{-13})
112	(0.83646, -0.10645×10^{-1})	(−0.87715, 0.96949×10^{-2})	(−0.87715, 0.96949×10^{-2})	(-0.14247×10^{-13}, 0.16456×10^{-13})

size parameter $x=80$; $m=(1.05, 0.005)$; $z=(84.0, 0.4)$; $N_{stop}=99$

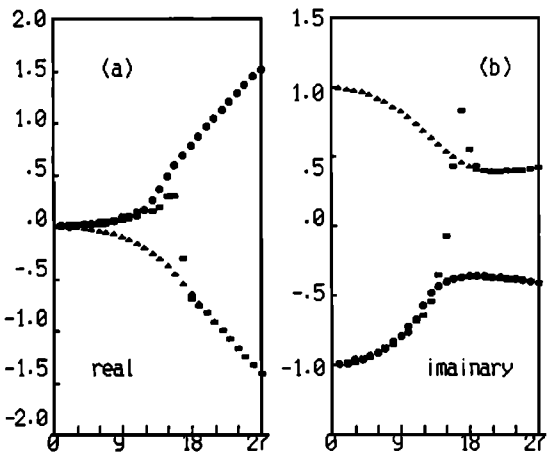

Fig. 2. $D_n^{(1)}(z)$ (dothed line), $D_n^{(2)}(z)$ (dashed line) and $D_n^{(3)}(z)$ (triangled line) versus n, (*a*) the real part, and (*b*) the imaginary part; the size parameter $z=(15.079, 2.953)$.

for 1 mm wavelength (at temperature of 273K) $m_2=(2.4, 0.47)$. The refractive index of ice is weakly dependent on frequecy, $m_1\approx 1.78$. Figure 2 shows $D_n^{(l)}(z)$ ($l=1$, 2, and 3) of water with $z=(15.08, 2.953)$. In these examples, $D_n^{(l)}(z)$ is computed using downward recursion, while the remnant logarithmic derivatives of Ricatti–Bessel functions and the ratio of spherical Bessel and Neumann functions are computed using upward recursion. When $n<|z|$, the above functions show an oscillatory behavior to some degree for small n, which depends on the argument z. This property is remakable as $|z|$ is large. Obviously, $D_n^{(2)}(z)=D_n^{(3)}(z)\approx -D_n^{(1)}(z)\approx -n/z$ as $n>N_{stop}$, and the ratio $\psi_n(z)/\xi_n(z)$ falls rapidly with increasing n.

We shall examine the asymptotic behavior and determine how the errors propagate when using (28) in upward recursion. It is a simple and important fact that the ratio $\psi_n(z)/\chi_n(z)$, including the ratio $\psi_n(z)/\xi_n(z)$, is bounded and the recursion is stable whenever the argument is any complex. Suppose an error ε_{n-1} is introduced and from (28) or (30) this error can be written as

$$\varepsilon_n=\varepsilon_{n-1}\cdot\left[\frac{D_n^{(j)}(z)+n/z}{D_n^{(1)}(z)+n/z}\right] \quad (j=2, 3) \quad (35)$$

When $D_n^{(1)}(z)$ and $D_n^{(j)}(z)$ ($j=2,3$) are computed by using downward and upward recurrence, respectively, the modules of the term in the bracket of (35) is less than unity for $n>z$. With increasing n the errors in $\psi_n(z)/\chi_n(z)$ and $\psi_n(z)/\xi_n(z)$ do not grow. Therefore $\psi_n(z)/\chi_n(z)$ and $\psi_n(z)/\xi_n(z)$ are calculated by using iterative formula (28) and (30), respectively. Both the real and the imaginary parts fall rapidly and tend to very small values close to zero as $n>N_{stop}$. The asymptotic behavior of $\psi_n(z)/\chi_n(z)$ is shown in Table 2 and in Figure 3. Of course, the converging speed for $\psi_n(z)/\chi_n(z)$ depends mainly on the argument. The converging property and asymptotic behaviour of $\psi_n(z)/\xi_n(z)$ are similar to those of $\psi_n(z)/\chi_n(z)$, which are shown in Table 1 and in Figure 3*a*.

Figure 3*a* shows the numerical results of $\psi_n(mx)/\chi_n(mx)$ and $\psi_n(mx)/\xi_n(mx)$ for core with $x_1=$

TABLE 2. The Asymptohc Be havior of $\psi_n(z)/\chi_n(z)$

$n \backslash z$	1.0	(18.487, 2.292)	(84.0, 0.4)	88.58
0	$0.15574\times10^{+1}$	$(-0.13366\times10^{-1}, 0.98473)$	(−0.78997, 0.70356)	0.70699
3	0.54115×10^{-3}	$(0.19454\times10^{-2}, 0.10223\times10^{+1})$	(0.78608, 0.69901)	$-0.12287\times10^{+1}$
7	0.34105×10^{-11}	$(-0.21938\times10^{-1}, 0.98013)$	$(0.10685\times10^{+1}, 0.11379\times10^{+1})$	−0.74319
15	0.81497×10^{-33}	$(-0.49398\times10^{-1}, 0.11462\times10^{-1})$	(−0.95712, 0.88684)	0.42599
24		$(-0.10124\times10^{-2}, -0.10598\times10^{-2})$	(−0.32730, 0.41098)	$0.12157\times10^{+1}$
30		$(-.17019\times10^{-7}, -0.53852\times10^{-6})$	$(-0.42091, 0.27315\times10^{+1})$	$-0.38200\times10^{+1}$
37		$(-0.16029\times10^{-15}, 0.77283\times10^{-15})$	(−0.14267, 0.35136)	$0.10772\times10^{+1}$
50			(−0.89897, 0.61820)	−0.27226
90			$(0.14608\times10^{-1}, 0.47156\times10^{-2})$	0.25325
99			$(0.16939\times10^{-5}, 0.94077\times10^{-6})$	0.36341×10^{-3}
105			$(0.64724\times10^{-5}, 0.44995\times10^{-5})$	0.49024×10^{-6}
110			$(0.38070\times10^{-12}, 0.31012\times10^{-12})$	0.74074×10^{-15}
120				0.37881×10^{-15}
N_{stop}	7	24	99	105

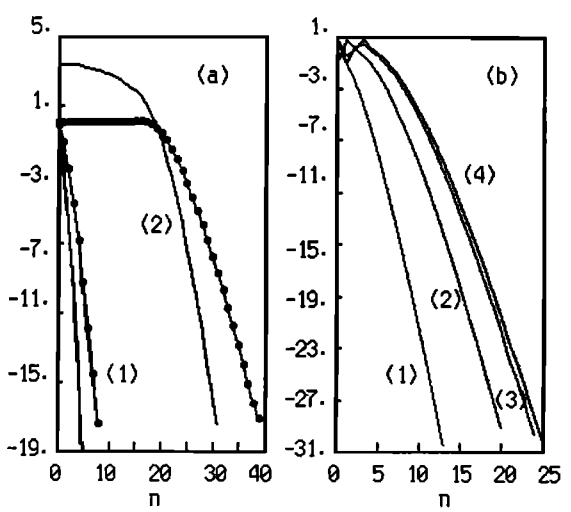

Fig. 3. (*a*) The logarithms of modules of $\psi_n(mx)/\chi_n(mx)$ (dotled line) and $\psi_n(mx)/\xi_n(mx)$ (solid line) versus n for a coated sphere. 1, core with $x_1 = 0.358$, $m_1 = (1.59, 0.66)$; 2, coat with $x_2 = 13.121$, $m_2 = (1.409, 0.1747)$. (*b*) The logarithms of modules of $\psi_n(mx)/\chi_n(mx)$ versus n for 1, the core; 2, the 16th; 3, the 48th; and 4, the 64th layer of an 80−layer sphere. (See equation (36)).

0.358, $m_1 = (1.59, 0.66)$ and for coat with $x_2 = 13.121$, $m_2 = (1.409, 0.1747)$. The corresponding ratio $\psi_n(x_2)/\xi_n(x_2)$ and $s = a_n + b_n$ are illustrated in Figure 4. The numerical results for angular distribution of scattering intensity and cross sections are accurately identical with those presented by *Bohren and Huffman* [1983].

Another example is an inhomogeneous sphere, in which refractive index profile is expressed as

$$m = (10.0/x - 1)^{1/2} \tag{36}$$

where x is the size parameter associated with the radius of the sphere. It is approximated by an 80−layer discrete sphere. The numerical results of $\psi_n(mx)/\chi_n(mx)$ for core, 16th, 48th, and 64th regions are illustrated in Figure 3*b*, and the corresponding size parameters are $x_1 = 0.757$, $x_{16} = 3.00$, $x_{48} = 4.584$, and $x_{64} = 4.90$, respectively. In general, the converging speed for ratio $\psi_n(z)/\chi_n(z)$ in inner spherical regions is greater than those associated with the outer regions, unless the size parameter of the inner region is larger.

5. SCATTERING COEFFICIENTS a_n AND b_n

In connection with the computation of various cross sections and the scattering intensity the scattering co-

efficients a_n and b_n are calculated from the analytic expressions of the type given in the preceding sections. We formulate a procedure for the calculation of a_n and b_n in the general case of a multilayered sphere with a numerical stable manner. Our procedure involves only three logarithmic derivatives of Ricatti–Bessel functions and ratios of spherical Bessel and Neumann functions. Our programs are written in the FORTRAN language standard on the IBM PC/XT/AT series of computers. The programs run on these computers under the MS–DOS operating system.

In (18)–(21), $A_n^{(j)}$ and $B_n^{(j)}$ depend on the size parameters and the refractive indices from the core to the jth–layered region, and are similar in form to the scattering coefficients for a homogeneous sphere with size parameter z. We have to discuss their asymptotic behavior, because with our computing procedure the size parameters $|m_j x_j|$ in most of the inner regions for a multilayered sphere are less than N_{stop}.

When order term n is appreciably larger than size parameter $|m_j x_j|$ of the jth region, from the analysis in the preceding section, $D_n^{(2)}(m_j x_{j-1}) \approx -D_n^{(1)}(m_j x_{j-1})$ and $\psi_n(m_j x_{j-1})/\chi_n(m_j x_{j-1})$ tends to a very small value close to zero. Thus $A_n^{(j)}$ and $B_n^{(j)}$ approximate to

$$A_n^{(j)} \approx B_n^{(j)} \leqslant \psi_n(m_j x_{j-1})/\chi_n(m_j x_{j-1})$$

and also approach zero. When $n > |m_j x_j|$, the size parameters and refractive indices in the outer regions have a remakable influence on calculation of the scattering coefficients a_n and b_n.

The modules of real and imaginary parts of the scattering coefficients decrease rapidly with increasing n, and $a_n \approx b_n$ when $n \gg |x_t|$. Their converging speeds are approximately the same as that of the ratio $\psi_n(x_t)/\xi_n(x_t)$ in order of magnitude. Let $s = a_n + b_n$ for any absorbing or nonabsorbing multilayered sphere. The curves s and $\psi_n(x_t)/\xi_n(x_t)$ are shown in Figure 4. From the figure one can see that s curves go rapidly down to a very small value as $n \gg |x_t|$ (to be more precise, $n \geqslant N_{stop}$).

Therefore the contributions from the outer spherical regions (or regions corresponding to a larger size parameter) to the scattering coefficients are greater than those associated with the inner regions (or regions of a smaller size parameter). And the contributions from all regions in a multilayered sphere play an important role in the scattering coefficients, only when n is smaller.

Our recursive algorithms are more stable and accurate in comparision with those for using directly Kerker's equations. First, Kerker's equations for a_n and b_n contain three Ricatti–Bessel functions and their derivatives, whose magnitudes may exceed the limit of any computer, because these functions are not bounded for a large and absorbing particle. This phenomena also occurs for a single sphere [*Fenn and Oser*, 1965; *Dave*, 1969; *Kattawar and Plass*, 1967; *Wiscome*, 1980; *Toon and Ackerman*, 1981]. For example,

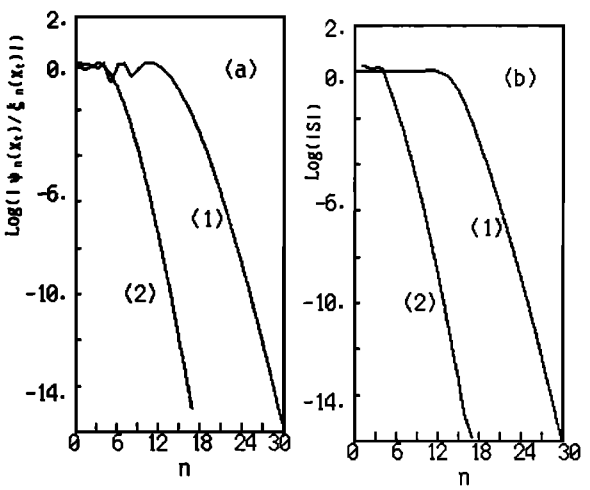

Fig. 4. (*a*) $|\psi_n(x_t)/\xi_n(x_t)|$ versus n and (*b*) $|s|$ versus n. in the Figures 4*a* and 4*b* curve 1 is the coated sphere, the same as Figure 3*a*; and curve 2 is an 80–layer sphere, (see equation (36)).

$$\chi_0(z) = \cos(x + iy) \tag{37a}$$

$$\chi_0(z) = 1/2 \cdot (\cos x - i\sin x)[\exp(y) + \exp(-y)] \tag{37b}$$

The magnitude increases exponentialy with the argument. Although the zero–order function may not exceed the limit of a computer, the higher–order functions computed by upward recurrence might. For example, let us check the function $\chi_n(z)$. When z is a single–precision variable, for $z = (10., 80.)$ the values of $\chi_n(z)$ overflow as $n > 69$. If z is a double–precision variable, for $z = (10, 600)$ these functions overflow as $n > 430$. When the function $\psi_n(z)$ is computed by using the method presented by *Abramowitz and Stegun* [1964], the similar problem also occurs. But our iteative equations replace the Ricatti–Bessel functios with their logathmic derivatives, whose calculational values are more stable and accurate and do not exceed the limit of any computer. Second, the ratios of Ricatti–Bessel functions $\psi_n(z)/\chi_n(z)$ and $\psi_n(z)/\xi_n(z)$ are bounded both for large values of size parameters and for a small value of the core radius. They converge rapidly with increasing n. Their fractional errors are independent of n and do not propagate. Third, in the case of a multilayered sphere the difference between the elements in determinants of Kerker's equations for a_n and b_n may be considerably large in order of magnitude when layer number t and total size parameter x_t are lar-

ger. More specifically, when order term n is large, the elements in rows of the determinants, which correspond to the inner regions of a multilayered sphere, have very small values close to zero. The problems associated with numerical round–off and accumulative errors may arise and the determinantal equations become ill conditioned. Our code avoids the above numerical instability and ill condition and is faster and more economical for computer storage. Finally, our iterative equations for a_n and b_n, (18)–(21), are similar in form to those for Mie theory for a homogeneous sphere. They reduce easily the expressions to a double–layered sphere and a single–layered sphere.

6. CALCULATION AND TEST OF THE ALGORITHM

On the basis of the analyses given in the preceding sections, the downward recurrence formula for $D_n^{(1)}(z)$ is used and the remnant parts are calculated using upward recursion in our computing procedure, and the tests of our procedures are performed. We have calculated various cross sections and the scattering intensity of the coated sphere and multilayered sphere given by other references [*Kerker*, 1969; *Bohren and Huffman*, 1983] and made a comparision, which indicates that both results are the same.

The scattering of the water–coated carbon sphere is illustrated in Figure 5, where extinction coefficient Qe, scattering coefficient Qs and absorption coefficient Qa are shown as functions of the total size parameter kb, when the ratio of the inner to outer radius is $q = a/b = 0.833$, the refractive indices of the core and coated regions are $m_1 = (1.59, 0.66)$ and $m_2 = 1.33$, respectively. The numerical results are compared with the corresponding results by using the determinantal form of Kerker's equations. The values calculated by using directly Kerker's equations are plotted as solid dots and are quite the same as those by the iterative algorithms.

Another example of considerable interest is the scattering of an ice surrounded by a water coating for the milliwave region. Their radius $a = 0.8$mm and $b = 1.0$ mm, and the refractive indices $m_1 = (1.78, 0.0024)$ and $m_2 = (2.4, 0.47)$ for $\lambda = 1$mm. The angular intensities i_V and i_H are illustrated in Figure 6 and compared with those for homogeneous ice and water spheres of the same outer size. When $q = a/b = 0.8$, the water–coated ice particle behaves essentially as if it consists only of the coating material and the main effect of coating is to decrease the backscattering.

We have also calculated the scattered field by an inhomogeneous sphere, whose refractive index profile is the Cauchy distribution [*Kerker*, 1969].

$$m = \beta / (1 + \varepsilon r^2 / b^2) \tag{38}$$

where b is the radius, and β and ε are real and positive constants. This distribution was approximated by a 50–layer discrete sphere. The numerical results are given in Figure 7, where a and b show the angular distribution of the scattered intensity and the degree of polarization for the incident unpolarized light, when the size parameter of the total sphere $kb = 5.0$ and refractive index of the surronding medium $m_s = 1.0$.

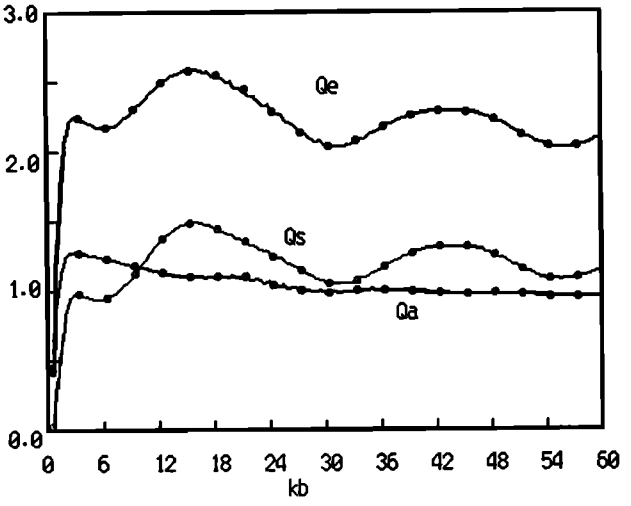

Fig. 5. Efficiencies for extinction, scattering, and absorption (Qe, Qs, Qa) for a water–coated carbon sphere.

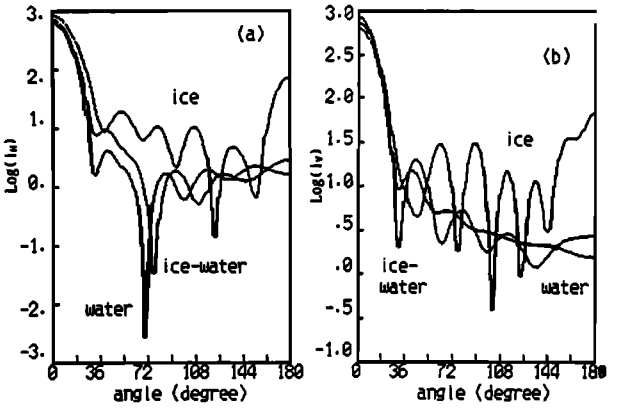

Fig. 6. Angular scattering by water–coated ice sphere and homogeneous water and ice spheres of the size. (*a*) parallel (i_H), and (*b*) perpendicular polarization (i_V).

Several tests were performed. We calculated various cross sections and the scattering intensity of a single homogeneous and a coated sphere for different refractive indices and size parameters. The numerical results are in good agreement with those by using the schemes presented by *Kattawar and Hood* [1967], *Wiscombe* [1980], *Toon and Ackerman* [1981]. In addition, the tests were done for values of size parameter x of a homogeneous sphere between 0.001 to 2000 for different complex

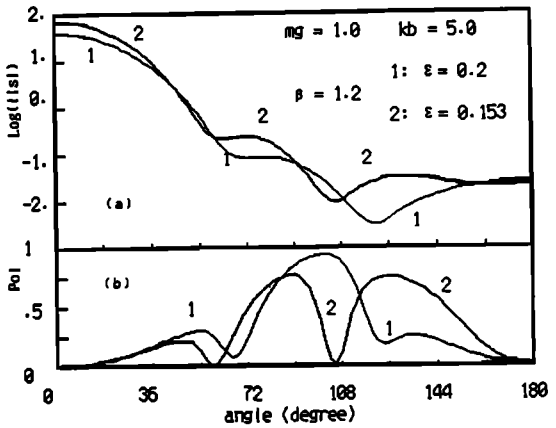

Fig. 7. (*a*) Angular distribution of scattering intensity and (*b*) the degree of polarazation.

refractive indices. The tests include setting the refractive indices of the core and shell to be equal and setting the core radius to be zero. In particular, large values of size parameters would cause numerical difficulties when Kerker's equations are in the form of determinants. But the equations presented in this paper and our complete computer procedure avoid these errors and is numericaly stable and accurate. Some important applications of them would be expected.

Acknowledgment. This work was supported by the National Natural Science Foundation of China.

REFERENCES

Abramowitz, M., and I. A. Stegum (Eds.), *Handbook of Mathematical Functions*, National Bureau of Standards, Washington, D. C., 1964.

Aden, A. L. and M. Kerker, Scattering of electromagnetic wave from concentric sphere, *J. Appl. Phys.*, 22, 1242–1246, 1951.

Bhandari, R., Scattering coefficients for a multilayered sphere: Analytic expressions and algorithms, *Appl. Opt.*, 24, 1960–1967, 1985.

Bohren, C. F. and D. R., Huffman, *Absorption and Scattering of Light by Small Particle*, Wiley–Interscience, New York, 1983.

Dave, J. V., Subroutine for computing the parameters of electromagnetic radiation scattered by a sphere, *Rep.* 320–3237, IBM, Sci. Cent., Palo Alto, Calif., 1968.

Dave, J. V., Scattering of visible light by large water sphere, *Appl. Opt.*, 8, 155, 1969.

Fenn, R. W., and H. Oser., Scattering properties of concentric soot–water sphere for visible and infrared light, *Appl. Opt.* 4, 1504–1509, 1965.

Kattawar, G. W., and G. N. Plass, Electromagnetic scattering from absorbing spheres, *Appl. Opt.*, 6, 1377 1382, 1967.

Kerker, M., *The Scattering of Light and Other Electromagnetic Radiation*, Academic, San Diegon, Calif., 1969.

Stratton, J. A., *Electromagnetic Theory*, McGraw–Hill, New York, 1941.

Toon, O. B., and T. P. Ackerman, Algorithms for the calculation of scattering by stratifield sphere, *Appl. Opt.*, 20, 3657–3660, 1981.

Wiscombe, W. J., Improved Mie scattering algorithms, *Appl. Opt.*, 19, 1505–1509, 1980.

Y. P. Wang and Z. S. Wu, Physics Department, Box 274, Xidian University, Xi'an, Shaanxi, People's Republic of China.